Pinning and unbinding of ideal polymers from a wedge corner

Pinning and unbinding of ideal polymers from a wedge corner

Raz Halifa Levi,[1,*] Yacov Kantor,[1] and Mehran Kardar[2]
[1]*Raymond and Beverly Sackler School of Physics and Astronomy, Tel Aviv University, Tel Aviv 69978, Israel*
[2]*Department of Physics, Massachusetts Institute of Technology, Cambridge, Massachusetts 02139, USA*
(Received 12 October 2017; published 19 December 2017)

A polymer repelled by unfavorable interactions with a uniform flat surface may still be pinned to attractive edges and corners. This is demonstrated by considering adsorption of a two-dimensional ideal polymer to an attractive corner of a repulsive wedge. The well-known mapping between the statistical mechanics of an ideal polymer and the quantum problem of a particle in a potential is then used to analyze the singular behavior of the unbinding transition of the polymer. The divergence of the localization length is found to be governed by an exponent that varies continuously with the angle (when reflex). Numerical treatment of the discrete (lattice) version of such an adsorption problem confirms this behavior.

DOI: 10.1103/PhysRevE.96.062132

I. INTRODUCTION

Absorption of polymers to surfaces is a common phenomenon, manifesting a competition between energy gain of binding and entropy loss of fluctuations in unbound configurations. As compromise, a polymer attached ("anchored") by one end to the surface may decrease its energy by staying within a finite distance ξ from the surface and frequently visiting it. The reduction in entropy of the polymer in this *absorbed* state is thus compensated by a bigger gain in energy; the balance between the two is determined by temperature T. Above the *adsorption critical temperature* T_a, the polymer depins from the surface, transitioning into a *delocalized* state. Such transitions have been studied in great detail in the literature [1–9].

Polymers in the bulk also exist in different states, with distinct universal characteristics [10]. Configurations of polymers in good solvents are designated as *self-avoiding*, with repulsive interactions between the monomers paramount. If the latter can be ignored, the polymers are called *ideal* and frequently modeled as random walks on a lattice. These, and other polymer types, each exhibit separate singular behavior near the adsorption transition, characterized by distinct exponents [11]. Transitions of *ideal* polymers have been extensively studied due to their analogy to well-known models of quantum particles in attractive potentials [12]. For most studies of adsorption transitions, the analogous potential includes both attractive areas and repulsive components, to model solid surfaces covered by an attractive layer. (In the absence of the repulsive part, an ideal polymer is always absorbed to an attractive layer.)

Geometry and dimensionality play an important role in determining the unbinding transition temperature and its singular behavior, leading to different characteristics for polymer adsorption to a rod [13,14], a sphere [15,16], or an arbitrarily shaped mesoscopic particle covered by an attractive layer [17]. In many cases, the adsorbing body introduces an external *length scale* to the polymer problem, through its finite size or curvature. However, there are also interesting cases where adsorption is to a *scale-free* form, such as the repulsive (infinite) wedge depicted in Fig. 1, with its edge covered by an attractive layer of microscopic diameter. A polymer attached to such a wedge is expected to undergo an adsorption transition with properties, including critical exponents, that depend on dimensionless descriptors such as the wedge angle. Such angle dependence of critical exponents is not new. The total partition function of a long flexible homogeneous polymer in a dilute solvent scales with the number of monomers N as $\mathcal{Z}_{\rm tot} \sim \mu^N N^{\gamma-1}$. While the leading (exponential) term depends on the nonuniversal parameter μ, the exponent γ in the subleading power law is universal depending on only a few major features, such as the space dimension d or the polymer state [10]. If a polymer is attached to a repulsive *scale-free* surface, such as a plane, or the tip of a cone or a wedge, its partition function will have the same form, but with a smaller exponent γ due to reduction in the number of possible configurations [18–20]. Similar behavior, albeit with a yet different set of angle-dependent exponents γ, is expected at the desorption transition from scale-free surfaces [21].

The *ideal* polymer in the configuration depicted in Fig. 1 maps to the quantum problem of a particle in the two-dimensional potential obtained from a cross section of the geometry. As we demonstrate in this work, this problem is exactly solvable. While different from the case of a realistic (hence self-avoiding) polymer in three dimensions, we hope that the two share qualitative characteristics. If the quality of a solvent is reduced, the monomers will tend to aggregate. At the compensation point between good and poor solvent, denoted the Θ point, the resulting polymer configurations are called Θ polymers [10]. In $d = 3$ in *free space* many of their characteristics are close to ideal polymers. However, we do not expect this similarity to extend to adsorption to a line. (The two-dimensional problem of a self-avoiding and Θ polymers in a similar potential does not have a bound state due to the screening of the attractive point.) We expect *self-avoiding polymers* and ideal polymers in the setup of Fig. 1 to share the property of continuous variations of exponents of the unbinding transition with the wedge angle, although the actual exponents will naturally differ.

The remainder of the paper is organized as follows: In Sec. II we recount the analogy between a polymer in the presence of a weak, slowly varying, potential, and the quantum mechanical problem of a particle in a potential well. We also

*razhalifa@gmail.com

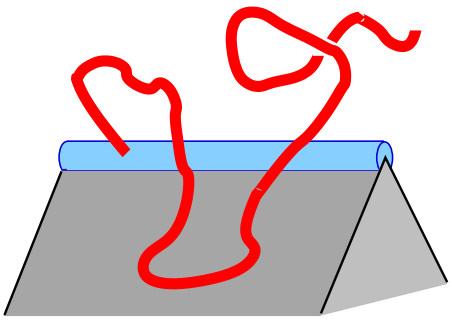

FIG. 1. Polymer (red) attached to a repulsive wedge (gray surface) with an attractive edge (blue). The wedge is assumed to be infinite.

formulate the problem on a lattice and point out the differences between continuous and discrete systems. In Sec. III we consider a two-dimensional problem of a circular well confined by the repulsive walls of a wedge. We find the critical strength of the well potential as a function of the wedge opening angle and characterize the singular behavior of the unbinding transition. The dependence on polymer length N and the exponent γ are detailed in Sec. IV. The discrete version of the problem, with an attractive lattice site located near a wedge is described in Sec. V, where we determine numerically both the transition point and the correlation length exponent for several wedge angles (Sec. VI).

II. ANALOGY TO QUANTUM BOUND STATES

The well-known mapping between adsorption of a polymer and bound states in quantum mechanics [12] is briefly reviewed here. Let $\mathcal{Z}(\mathbf{r},\mathbf{r}_0,N)$ denote the partition function of an ideal polymer of N steps, of mean squared size ℓ^2, that starts at point $\mathbf{r}_0$ and ends at point $\mathbf{r}$. In free space the total partition function is $\mathcal{Z}_0 \equiv \int \mathcal{Z} \mathrm{d}^d\mathbf{r} = \mu^N$, and it is convenient to define the *reduced* partition function $\tilde{\mathcal{Z}}(\mathbf{r},\mathbf{r}_0,N) = \mathcal{Z}(\mathbf{r},\mathbf{r}_0,N)/\mathcal{Z}_0$. If the potential affecting the monomers, $V^{\rm th}(\mathbf{r})$, changes slowly, such that at temperature T its change over the distance ℓ is much smaller than $k_BT \equiv \beta^{-1}$, then the partition function difference $\tilde{\mathcal{Z}}(\mathbf{r},\mathbf{r}_0,N+1) - \tilde{\mathcal{Z}}(\mathbf{r},\mathbf{r}_0,N) \approx \partial\tilde{\mathcal{Z}}/\partial N$ can be cast in the continuum form [22]

$$\frac{\partial\tilde{\mathcal{Z}}}{\partial N} = \frac{\ell^2}{2d}\nabla^2\tilde{\mathcal{Z}} - \beta V^{\rm th}\tilde{\mathcal{Z}}, \tag{1}$$

supplemented with the initial condition $\tilde{\mathcal{Z}}(\mathbf{r},\mathbf{r}_0,0) = \delta^d(\mathbf{r}-\mathbf{r}_0)$. This equation can be solved by variable separation, which leads to eigenvalue equation

$$\left(-\frac{\ell^2}{2d}\nabla^2 + \beta V^{\rm th}\right) f_\alpha = E_\alpha^{\rm th} f_\alpha. \tag{2}$$

Knowledge of all the eigenfunctions f_α, and their eigenvalues ("energies") $E_\alpha^{\rm th}$, enables reconstruction of the reduced partition function as

$$\tilde{\mathcal{Z}}(\mathbf{r},\mathbf{r}_0,N) = \sum_\alpha f_\alpha(\mathbf{r}) f_\alpha^*(\mathbf{r}_0) \mathrm{e}^{-E_\alpha^{\rm th} N}. \tag{3}$$

The analogy of the above treatment with the single particle Schrödinger equation is immediately apparent. In this analogy, the variable N corresponds to an imaginary time for the quantum particle, its mass m and potential $V^{\rm q}$ related by $\beta V^{\rm th} d/\ell^2 = mV^{\rm q}/\hbar^2$, with the same scaling for E_αs in the eigenvalue equation.

If the potential $V^{\rm th}(\mathbf{r})$ includes attractive parts, it may support bound states [23] with discrete eigenvalues $E_\alpha^{\rm th} < 0$. If there is a gap between the ground and the first excited state, for large N the solution will be dominated by the ground state ($\alpha = 0$), and

$$\tilde{\mathcal{Z}}(\mathbf{r},\mathbf{r}_0,N) \approx f_0(\mathbf{r}) f_0(\mathbf{r}_0) \mathrm{e}^{-E_0^{\rm th} N}. \tag{4}$$

Since $\tilde{\mathcal{Z}}$ is positive, the ground state function $f_0(\mathbf{r})$ cannot alternate in sign, and can be chosen as being non-negative everywhere. (The absence of nodes in the ground state of a quantum particle is well known.) A bound state $f_0(\mathbf{r})$ will be localized within some localization length ξ in the neighborhood of the well. Since $\tilde{\mathcal{Z}}$ is proportional to the probability to find the polymer end at $\mathbf{r}$, this implies that the polymer is also localized in the vicinity of the attractive potential. Assuming a typical linear size a of the potential "well," it is convenient to recast the equation in terms of dimensionless coordinates $\mathbf{r}' = \mathbf{r}/a$, as

$$(-\nabla'^2 + V) f_\alpha = E_\alpha f_\alpha. \tag{5}$$

Here ∇'^2 represents the Laplacian in dimensionless coordinates, $E_\alpha \equiv (2a^2 d/\ell^2) E_\alpha^{\rm th}$ are the dimensionless energy eigenvalues, and

$$V \equiv \frac{2d\beta a^2}{\ell^2} V^{\rm th} \tag{6}$$

is the dimensionless potential. For further reference, we note that the N-dependent Eq. (1) in the new dimensionless variables can be expressed as

$$\frac{\partial\tilde{\mathcal{Z}}}{\partial N'} = \nabla'^2\tilde{\mathcal{Z}} - V\tilde{\mathcal{Z}}, \tag{7}$$

where $N' \equiv N\ell^2/(2da^2)$. Note that $E_\alpha N' = E_\alpha^{\rm th} N$. In what follows, we omit the prime in coordinate notation and always measure the distances relative to the extent of the potential.

It is well known in quantum mechanics that any purely attractive potential in $d = 1$ dimension always has a bound state [24], while a sufficiently deep well may have many bound states. (There is also a slightly more relaxed criterion guaranteeing the presence of bound states [25].) The situation is similar in $d = 2$ dimensions, where a bound state can always be found [26]. As a concrete example, consider a circular well of unit radius

$$V_{\rm circ}(\mathbf{r}) = \begin{cases} -V_0, & \text{for } r < 1 \\ 0, & \text{for } r \geqslant 1 \end{cases}. \tag{8}$$

The above discontinuous potential was chosen for its simplicity, since we expect that the universal features of the unbinding transition are independent of its detailed shape (as is the case in $d = 1$). This choice may appear to contradict the statement at the beginning of this section that the analogy of the ideal polymer to the "quantum particle" in Eq. (1) is valid only for slowly varying potentials. The actual requirement is that for a potential $V^{\rm th} \sim k_BT$ the range Δr of the change in the potential should satisfy $\ell \ll \Delta r$. The discontinuous potential

in Eq. (8) can thus be viewed as the continuum limit of the case of $\ell \ll \Delta r \ll a = 1$ and therefore represents a valid situation for this mapping.

The eigenfunctions in both interior and exterior of the well described by Eq. (8) are Bessel functions. In the case of the ground state they correspond to the regular and second modified Bessel functions J_0 and K_0, respectively. For a shallow well ($V_0 \ll 1$) the ground state energy is extremely small ($E_0 \sim \mathrm{e}^{-4/V_0}$), and the corresponding localization length is very large [27]. In higher dimensions d, the presence or absence of bound states depends on the depth and details of the potential. In fact, if d is viewed as continuous variable, it can be shown [27] that the property of always having a bound state disappears immediately above $d = 2$.

The above theorems do not apply to potentials that have both repulsive and attractive parts. For instance, a one-dimensional potential representing an attractive layer on a repulsive wall may have no bound states if it is shallow enough. We shall see that a similar situation appears for a two-dimensional circular well in the presence of repulsive walls.

Many theoretical studies of polymers near attractive and repulsive surfaces are performed on discrete lattice models. We will consider a d-dimensional hypercubic lattice, with lattice spacing ℓ, with polymer configurations represented by N-step walks. The total partition function of a polymer in the absence of any potentials is $\mathcal{Z}_0 = (2d)^N$. The potential V^{th} is modeled by Boltzmann weights $q(\mathbf{r}) = \exp(-\beta V^{\mathrm{th}})$ assigned to lattice sites. In free space $q = 1$, on the repulsive wall $q = 0$, while for well of depth $V^{\mathrm{th}} = -V_0^{\mathrm{th}}$, $v = \exp(\beta V_0^{\mathrm{th}})$. The reduced $(N+1)$-step partition function can be deduced from N-step reduced partition function by

$$\tilde{\mathcal{Z}}(\mathbf{r},\mathbf{r}_0,N+1) = \frac{q(\mathbf{r})}{2d} \sum_{\mathbf{r}' \text{ nn of } \mathbf{r}} \tilde{\mathcal{Z}}(\mathbf{r}',\mathbf{r}_0,N), \tag{9}$$

with the starting condition $\tilde{\mathcal{Z}}(\mathbf{r},\mathbf{r}_0,0) = q(\mathbf{r}_0)\delta_{\mathbf{r},\mathbf{r}_0}$.

As an aside, note that hypercubic lattices are bipartite, their sites separable into disjoint "even" ("e") and "odd" ("o") subsets. A walk starting on one subset lands on the same subset (or its complement) after an even (odd) number of steps, with $\tilde{\mathcal{Z}}(\mathbf{r},\mathbf{r}_0,N) = 0$ on one or other subset. Equation (9) can be written in matrix form

$$\tilde{\mathcal{Z}}_{N+1} = M\tilde{\mathcal{Z}}_N, \tag{10}$$

where the matrix $M(\mathbf{r},\mathbf{r}')$ connects "e" and "o" coordinates. A further recursion yields

$$\tilde{\mathcal{Z}}_{N+2} = M^2\tilde{\mathcal{Z}}_N, \tag{11}$$

which connects only sites of the same type. Thus the matrix M^2 can be decomposed into two completely unconnected submatrices. Since the elements of each submatrix are positive, the largest eigenvalue λ^2 is real positive, and the corresponding eigenvector is unique. Indicating by $\psi_{\mathrm{e}}(\mathbf{r})$ the eigenvector in the even subspace,

$$\lambda^2\psi_{\mathrm{e}}(\mathbf{r}) = M^2(\mathbf{r},\mathbf{r}')\psi_{\mathrm{e}}(\mathbf{r}'), \tag{12}$$

it is easy to see that $\psi_{\mathrm{o}}(\mathbf{r}) \equiv M(\mathbf{r},\mathbf{r}')\psi_{\mathrm{e}}(\mathbf{r}')$ is an eigenvector (with eigenvalue λ^2) in the odd subspace. The orthogonal states ψ_{o} and ψ_{e} are in the above sense "ground states" of the problem, with energy E_0 obtained from $\lambda^2 = \mathrm{e}^{-2E_0}$.

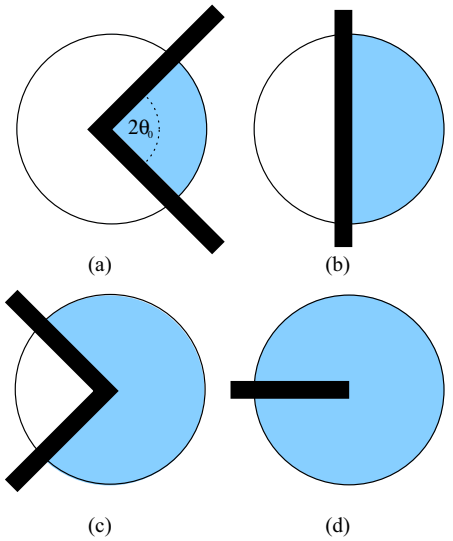

FIG. 2. Circular potential well (blue area) of radius 1 and depth $-V_0$, confined to a sector of opening angle $2\theta_0$ by hard walls. The subfigures represent examples of (a) inside a rectangular sector ($\theta_0 = \pi/4$), (b) near a flat surface (line) ($\theta_0 = \pi/2$), (c) outside a rectangular sector ($\theta_0 = 3\pi/4$), and (d) outside a needle-like sector ($\theta_0 = \pi$).

For a weak potential with small variations between adjacent lattice sites, Eq. (9) coincides with Eq. (1). However, in a typical lattice simulation the geometrical features are reduced to a bare minimum; e.g., an attractive well near a flat repulsive surface is represented by a *single* lattice layer of sites with some weight w, while a well near a repulsive wall or wedge may be represented by a single attractive site with a weight v. Since the width of the attractive layer, or a well a, coincide with the polymer step size ℓ, we may expect only qualitative similarity between the solutions of Eqs. (1) and (9). Nevertheless, we shall see that the results of continuous and discrete problems are rather close in their numerical values.

III. ATTRACTIVE CIRCULAR WELL WITHIN A SECTOR

We next consider a circular well, as in Eq. (8), near a repulsive wall, either flat or forming a sector with opening angle $2\theta_0$ as depicted in Fig. 2. The potential will be

$$V_{\mathrm{sect},\theta_0}(r,\phi) = \begin{cases} V_{\mathrm{circ}}(\mathbf{r}), & \text{for } -\theta_0 < \phi < \theta_0, \\ \infty, & \text{otherwise,} \end{cases} \tag{13}$$

where r and ϕ are the polar coordinates depicting the distance from the origin, and the azimuthal angle, respectively. As before, we assume that the distances are measured relative to the circle radius.

In polar coordinates, Eq. (5) for potential V_{sect} becomes

$$-\left[\frac{1}{r}\frac{\partial}{\partial r}\left(r\frac{\partial f_\alpha}{\partial r}\right) + \frac{1}{r^2}\frac{\partial^2 f_\alpha}{\partial \phi^2}\right] = \epsilon_\alpha f_\alpha, \tag{14}$$

where $\epsilon_\alpha \equiv E_\alpha + V_0$ inside the well ($r < 1$), and $\epsilon_\alpha \equiv E_\alpha$ outside the well ($r > 1$). The repulsive walls of the sector are enforced by the boundary condition $f_\alpha(r,\phi = \pm\theta_0) = 0$. The eigenfunction f_α and its derivative are continuous at $r = 1$. To ensure that the function vanishes on the boundaries of the sector, its angular dependence in constrained to the forms

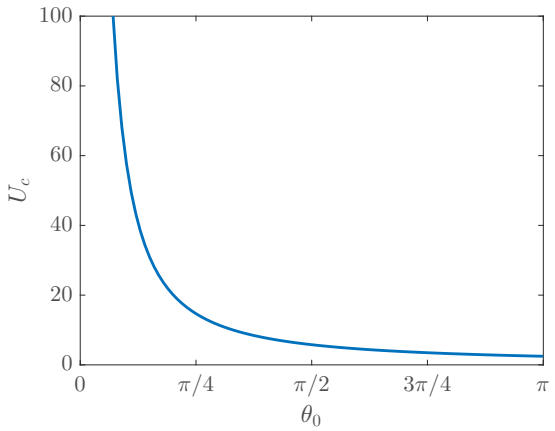

FIG. 3. Critical depth of a well U_c as a function of the half of the central angle θ_0 of the sector.

$\sin(\nu\phi)$, with $\nu = (\pi/\theta_0)n$, for $n = 1,2,\ldots$; or $\cos(\nu\phi)$, with $\nu = (\pi/\theta_0)(n+\frac{1}{2})$, for $n = 0,1,2,\ldots$. In general, ν is not an integer, except at $\theta_0 = \pi/2$, when the sector becomes a flat surface. Discrete eigenstates of a circular well with *infinite* walls, i.e., with $V = \infty$ for $r > 1$, confined by a sector were analyzed in detail in Ref. [28]. Our problem of a well of *finite* depth admits both discrete ($E_\alpha < 0$) and continuous ($E_\alpha \geqslant 0$) spectra. For $E_\alpha < 0$ the radial part of the solution is [29] a regular Bessel function $J_\nu(kr)$ with $k = \sqrt{E_\alpha + V_0}$ for $r < 1$, and second modified Bessel function $K_\nu(qr)$ with $q = \sqrt{-E_\alpha}$ for $r > 1$. This choice of the Bessel functions ensures regularity of the solution at $r = 0$ and its vanishing for $r \to \infty$. Since Eq. (5) is a *second order* linear equation, for *finite* potential V, the second derivative must exist, and consequently both the function and its derivative must be continuous. In the presence of the finite jump in V there is a *finite* jump in the *second* derivative, but the first derivative remains continuous as in the case of smooth V. Therefore, the eigenvalue E_α, should be selected to enforce continuity of the function and its derivative at $r = 1$. Thus E_α is a solution of the equation

$$\frac{kJ'_\nu(k)}{J_\nu(k)} = \frac{qK'_\nu(q)}{K_\nu(q)}, \tag{15}$$

where the prime denotes derivative of a function with respect to its argument. For large V_0 we can have multiple bound states for several values of ν.

Since we are interested in the ground state, we will consider only $\nu = m \equiv \pi/2\theta_0$, since larger ν solutions have alternating signs. Of all possible solutions for this m we look for the smallest k. The number of bound states will decrease with decreasing V_0, and for a limiting $V_0 = U_c$ the eigenenergy E_0 of the ground state is zero, reducing Eq. (15) to

$$\frac{\sqrt{U_c}J'_m(\sqrt{U_c})}{J_m(\sqrt{U_c})} = \lim_{q\to 0}\frac{qK'_m(q)}{K_m(q)} = -m. \tag{16}$$

By using the recurrence relations of Bessel functions and their derivatives [30], we find that Eq. (16) is reduced to solving $J_{m-1}(\sqrt{U_c}) = 0$. Thus, U_c is simply the square of the first zero of $J_{(\pi/2\theta_0)-1}$. Figure 3 depicts the dependence of U_c on the angle θ_0. As expected, the critical depth U_c diverges with increasing confinement for $\theta_0 \to 0$. Since for large m the first root of J_m is approximately at m [31], for small θ_0 we have $U_c \approx m^2 = (\pi/2\theta_0)^2$. At the other extreme $U_c(\theta_0 = \pi) = \pi^2/4$, while the radial part of the ground state eigenfunction at $E_0 = 0$ inside the well becomes $J_{1/2}(\pi r/2)$, where $J_{1/2}(x) \sim \sin(x)/\sqrt{x}$. Thus U_c remains finite when the sector becomes a needle-like insertion into the attractive well and the eigenfunction has a very different shape from the bound states of a circular well without the repulsive walls. For $\theta_0 = \pi/2$ the sector becomes a straight line, and $U_c \approx 5.78$.

For $V_0 > U_c$ bound states are present, and the partition function at large distances is described by $K_m(qr) \sim \sqrt{\frac{\pi}{2qr}}e^{-qr}$. The exponential decay of this function implies that the polymer is localized in the vicinity of the corner over a distance of order $\xi = 1/q = 1/\sqrt{-E_0}$. (For long polymers, only the ground state needs to be taken into account.) When $E_0 = 0$ the exponential long distance decay of $K_m(qr)$ is replaced by a power law r^{-m}. This is different from the one-dimensional case, where $E_0 = 0$ corresponds to a function that is constant outside the well. When the depth of the well is close to U_c, i.e., for small $\delta V_0 \equiv V_0 - U_c$, E_0 is also small, and we can expand the left-hand side of Eq. (15) (with $\nu = m$) $\mathcal{F}_{\mathrm{L},m}(k) = \mathcal{F}_{\mathrm{L},m}(\sqrt{U_c + \delta V_0 + E_0}) \equiv kJ'_m(k)/J_m(k)$ in $\delta V_0 + E_0$,

$$\mathcal{F}_{\mathrm{L},m} \approx -m - \tfrac{1}{2}(E_0 + \delta V_0), \tag{17}$$

and also expand the right-hand side of the same equation $\mathcal{F}_{\mathrm{R},m}(q) = \mathcal{F}_{\mathrm{R},m}(\sqrt{-E_0}) \equiv qK'_m(q)/K_m(q)$ in $(-E_0)$. The latter expansion has different forms depending on the value of $m = 2\theta_0/\pi$ [30]:

$$\mathcal{F}_{\mathrm{R},m} \approx \begin{cases} -m - \frac{1}{2(m-1)}(-E_0), & \text{for } m > 1, \\ -1 + \frac{1}{2}(-E_0)\ln(-E_0), & \text{for } m = 1, \\ -m - \frac{2^{1-2m}\pi}{\sin(\pi m)\Gamma^2(m)}(-E_0)^m, & \text{for } \frac{1}{2} \leqslant m < 1. \end{cases} \tag{18}$$

By equating $\mathcal{F}_{\mathrm{L},m} = \mathcal{F}_{\mathrm{R},m}$ we find that, to the leading order, E_0 depends on δV_0 as follows:

$$q^2 = -E_0 \sim \begin{cases} \delta V_0, & \text{for } 0 < \theta_0 < \frac{\pi}{2}, \\ \delta V_0/|\ln \delta V_0|, & \text{for } \theta_0 = \frac{\pi}{2}, \\ \delta V_0^{2\theta_0/\pi}, & \text{for } \frac{\pi}{2} < \theta_0 \leqslant \pi. \end{cases} \tag{19}$$

Since the dimensionless potential V_0 depends on the physical potential V_0^{th} and the temperature via Eq. (6), $\delta V_0 = (2a^2 d/k_B\ell^2)V_0^{\mathrm{th}}(1/T - 1/T_a) \approx (2a^2 d/k_B T_a^2 \ell^2)V_0^{\mathrm{th}}(T_a - T)$, we can relate the divergence of the localization length to the temperature difference by

$$\xi \sim \begin{cases} (T_a - T)^{-\frac{1}{2}}, & \text{for } 0 < \theta_0 < \frac{\pi}{2}, \\ |\ln(T_a - T)|^{\frac{1}{2}}(T_a - T)^{-\frac{1}{2}}, & \text{for } \theta_0 = \frac{\pi}{2}, \\ (T_a - T)^{-\frac{\theta_0}{\pi}}, & \text{for } \frac{\pi}{2} < \theta_0 \leqslant \pi. \end{cases} \tag{20}$$

In the above equation, T_a itself depends on θ_0 due to the θ_0 dependence of the critical depth U_c. The $\theta_0 \to \pi$ limit in the third case of Eq. (20) represents a needle-like insertion into the circular well and differs from the situation when the walls of the wedge are completely absent, since the semi-infinite straight line presents a significant obstacle for a random walk. The dependence of the critical behavior in Eq. (20) is reminiscent of other power-law dependencies, such as that of

the density of the polymer, or the pressure it exerts on walls of a wedge [32]. (In particular, see Fig. 5 in Ref. [32].) They are all manifestations of scale invariance of the geometry, and appropriate polymer properties. Detailed knowledge of the pressure distribution may shed light on the nontrivial behavior described by Eq. (20). The results in Ref. [32] are expected to be valid in the desorbed phase. The formalism presented in this paper does not allow direct calculation of the local pressure distribution. It is likely that other existing analytical and numerical, continuous space, and lattice methods [32–36] can be extended to calculations of pressure in the presence of attractive potentials.

Close to the transition point, and at very large distances $r \gg \xi$, the bound eigenstate has radial component $K_m(r/\xi) \sim e^{-r/\xi}\sqrt{\xi/r}$. However, for distances $a < r \ll \xi$, where $a = 1$ is the well radius in our calculations, the eigenstate has a simple power law dependence $\sim r^{-m}$. The "typical" polymer size is usually determined through an average of a power of end-to-end distance, such as $R^n \equiv \langle r^n \rangle$. However, whether or not this quantity reflects the localization length ξ depends on the powers n and m. The value of m also determines whether the relevant normalization is determined by ξ or a. Thus, for various cases we find

$$R^n \sim \begin{cases} \xi^n, & \text{for } m < 2, \\ \xi^n/\ln(\xi/a), & \text{for } m = 2, \\ \xi^{2-m+n}/a^{2-m}, & \text{for } 2 < m < 2+n, \\ a^n \ln(\xi/a), & \text{for } m = 2+n, \\ a^n, & \text{for } m > 2+n. \end{cases} \tag{21}$$

Close to the transition, the correlation length will be very large, and a sufficiently long polymer settles into the localized ground state, with measures of its size given by Eq. (21). However, for moderate values of N, the partition function will evolve as a Gaussian, i.e., it will have width of order of $\sqrt{N}$. In such a case, ξ in the above expressions should be replaced by $\sqrt{N}$.

IV. *N*-DEPENDENT SOLUTIONS INSIDE THE SECTOR

At very high temperatures the dimensionless potential V in Eq. (7) becomes negligible, reducing it to the simple diffusion equation

$$\frac{\partial \tilde{\mathcal{Z}}}{\partial N'} = \nabla^2 \tilde{\mathcal{Z}}, \tag{22}$$

where the rescaled polymer length N' plays the role of time. The required solution for $\tilde{\mathcal{Z}}$ must still vanish on the *repulsive* boundaries of the sector, corresponding to *absorbing* boundaries for the diffusers. The exact solution to this problem depends on the initial position of the diffuser (starting point of the polymer) $\mathbf{r}_0$. However, for sufficiently large $N' \gg r_0^2$, a significant portion of diffusing density will reach the boundary, and the memory of the initial condition is only reflected in the prefactor of the asymptotic solution [32,37]

$$\tilde{\mathcal{Z}}(\mathbf{r_0},\mathbf{r},N') = c\frac{r^m}{N'^{1+m}} e^{-r^2/4N'} \cos(m\phi). \tag{23}$$

As before, the angle ϕ is measured form the axis of symmetry and $m = \pi/2\theta_0$, while the prefactor c depends on $\mathbf{r_0}$. Integration of the reduced partition function leads to total partition function $\tilde{\mathcal{Z}}_{\rm tot} = \text{const}\, N'^{-m/2}$, and therefore exponent $\gamma = 1 - m/2 = 1 - \pi/4\theta_0$ [18–20].

The search for an N'-dependent solution of the diffusion equation in a wedge with absorbing boundaries (corresponding to repulsive surfaces for the polymer) revealed [32,37], that besides the solution in Eq. (23) there is a complementary solution

$$\tilde{\mathcal{Z}}(\mathbf{r_0},\mathbf{r},N') = \frac{c}{r^m N'^{1-m}} e^{-r^2/4N'} \cos(m\phi), \tag{24}$$

where the notations are the same as before. This, solution is not appropriate for a purely absorbing wedge, since it diverges as r^{-m} for $r \to 0$, and was thus discarded for the repulsive boundary problem in Refs. [32,37]. However, we note that such functional form resembles the ground state at the transition point for a polymer in a wedge with an attractive well. Unlike the true ground state, this solution has an N'-dependent prefactor and a Gaussian function that truncates the power law behavior, and is a candidate for the asymptotic N'-dependent solution for the reduced partition function outside the well (valid for sufficiently large N', when the details of the initial condition have been forgotten). We do not know the continuation of this function inside the well, but expect that it can be constructed by superposition of states. The fact that in the small r limit the logarithmic derivative $d\ln\tilde{\mathcal{Z}}/d\ln r \to -m$ indicates that this might be a general solution of a small and deep attractive region in the wedge at the transition temperature. We shall later verify this assumption by numerical solutions of discrete problems.

Assuming that Eq. (24) indeed correctly represents the reduced partition function, we can integrate the expression to obtain the total partition function $\tilde{\mathcal{Z}}_{\rm tot} = \text{const}\, N'^{\gamma-1}$, with

$$\gamma = \begin{cases} 1 + m/2, & \text{for } m < 2, \\ 2 \text{ (with log correction)}, & \text{for } m = 2, \\ m, & \text{for } m > 2. \end{cases} \tag{25}$$

These exponents are larger than 1, the value for free space, and therefore the mixture of repulsive wedge with critical attractive point at its corner corresponds to an overall attraction for a polymer in free space.

V. ATTRACTIVE POINT NEAR A REPULSIVE SECTOR ON A LATTICE

For numerical studies of polymer adsorption, discrete (lattice) models provide convenient realizations. Some simple discrete analogs for a small adsorbing well at the corner of a repulsive wedge are depicted in Fig. 4, with the attractive potential acting on a single point near a line of repulsive sites. Equation (9) provides a simple recursive numerical tool for calculating $\tilde{\mathcal{Z}}(\mathbf{r},\mathbf{r}_0,N+1)$ in terms of $\tilde{\mathcal{Z}}(\mathbf{r},\mathbf{r}_0,N)$: Starting with $\tilde{\mathcal{Z}}(\mathbf{r},\mathbf{r}_0,0) = q(\mathbf{r}_0)\delta_{\mathbf{r},\mathbf{r}_0}$, Eq. (9) is iterated N times for polymer length N. The resulting $\tilde{\mathcal{Z}}(\mathbf{r},\mathbf{r}_0,N)$ is proportional to the probability of finding the end of the polymer at $\mathbf{r}$. The total reduced partition function $\tilde{\mathcal{Z}}_{\rm tot}(\mathbf{r}_0,N) = \sum_{\mathbf{r}} \tilde{\mathcal{Z}}(\mathbf{r},\mathbf{r}_0,N)$ is the normalizing factor for this probability.

The total reduced partition function $\tilde{\mathcal{Z}}_{\rm tot}(\mathbf{r}_0,N)$ is, by definition, equal to one in free space. In the absence of attractive potential, a polymer near a repulsive sector will have partition function reduced to $\tilde{\mathcal{Z}}_{\rm tot} \sim N^{\gamma-1}$, where $\gamma = 1 - \pi/4\theta_0 < 1$

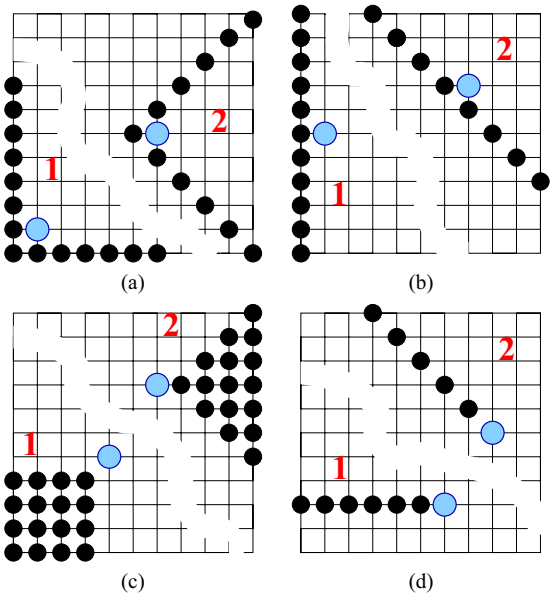

FIG. 4. Illustration of a single adsorbing point (light blue circle with Boltzmann weight $v > 1$), at a corner of a repulsive sector (black full circles with weight 0) on a square lattice. For each sector semiangle θ_0, two discrete variants of the continuous geometry (corresponding pictures in Fig. 2) are shown: "1" corresponds to straight lines along the lattice axes, and "2" along the lattice diagonals. The number of repulsive sites neighboring the adsorbing site, n, varies between the two variants. In panel (a) the attracting point inside the rectangular repulsive sector ($\theta_0 = \pi/4$) has $n_1 = 2$ nearest-neighbor repulsive sites in variant "1," and $n_2 = 3$ in "2." In panel (b), for the attracting point near a flat repulsive surface (line) ($\theta_0 = \pi/2$), $n_1 = 1$ and $n_2 = 2$. In panel (c), for the attracting point outside a rectangular repulsive sector ($\theta_0 = 3\pi/4$), $n_1 = 0$ and $n_2 = 1$. In panel (d), an attracting point at the tip of a semi-infinite repulsive line ($\theta_0 = \pi$), has $n_1 = 1$ and $n_2 = 0$.

depends on the wedge angle [18–20]. This behavior persists for a weakly attractive potential, with v close to 1. As v increases towards v_c, this scaling is delayed to larger values of N. In the adsorbed state $\tilde{\mathcal{Z}}_{\rm tot}$ will increase exponentially with N due to extra Boltzmann weights gained upon repeated returns to the attracting point. Again, the exponential growth, immediately apparent for $v \gg v_c$, is delayed to larger N as v is decreased towards v_c. Figure 5 depicts the dependence of $\tilde{\mathcal{Z}}_{\rm tot}$ for several values of v very close to v_c. Only for polymers of several thousand steps does it become evident that the two lowest graphs correspond to delocalized states, while the two top graphs, and possibly the middle one, represent adsorbed states.

If $\mathbf{r}_0$ is located at or near the attractive point, we can use the mean squared end-to-end distance

$$R^2(N) = \frac{1}{\tilde{\mathcal{Z}}_{\rm tot}(\mathbf{r}_0, N)} \sum_{\mathbf{r}} (\mathbf{r} - \mathbf{r}_0)^2 \tilde{\mathcal{Z}}(\mathbf{r}, \mathbf{r}_0, N) \qquad (26)$$

as an indicator of the localization length. In the absence of the attractive potential, the repulsive walls push away the polymer while maintaining the scaling of the random walk, such that for a polymer anchored close to the apex of a wedge $R^2 = N(1 + \pi/4\theta_0)$ [32,37]. (In this section distances are measured in units of lattice spacing, corresponding to $\ell = 1$.) This is

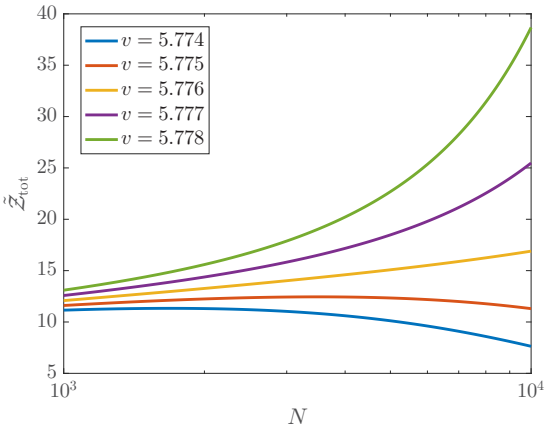

FIG. 5. Semilogarithmic plot of the dependence of the total reduced partition function $\tilde{\mathcal{Z}}_{\rm tot}$ on polymer length N for an attractive point located inside a rectangular wedge ($\theta_0 = \pi/4$), as depicted in Fig. 4(a) for geometry "1," for Boltzmann weights v ranging from 5.774 to 5.778 (bottom to top).

indeed the behavior observed for v close to 1. In an adsorbed state R^2 approaches a constant as N increases, masked by crossovers close to v_c. Figure 6 depicts R^2/N as a function of N for the same values of v is in Fig. 5. The two lowest curves in this figure, and possibly the middle one, correspond to adsorbed state, with the top graphs in delocalized states. From the last two figures we estimate that $v_c \approx 5.776$. Larger N will enable even more accurate determination of v_c.

The presence of an adsorption transition can easily be detected visually by inspecting the probability of the end point, proportional to $\tilde{Z}(\mathbf{r}, N)$. In the absence of the attractive site ($v = 1$), this probability density is a Gaussian multiplied by a power law as in Eq. (23). Figures 7(a) and 7(c) depict such situations for geometries of type "1" in Figs. 4(b) and 4(c), respectively. Even for a weakly attractive potential, i.e., for v somewhat larger than 1, the distribution of the polymer end point approaches such a form for large N. At the critical points

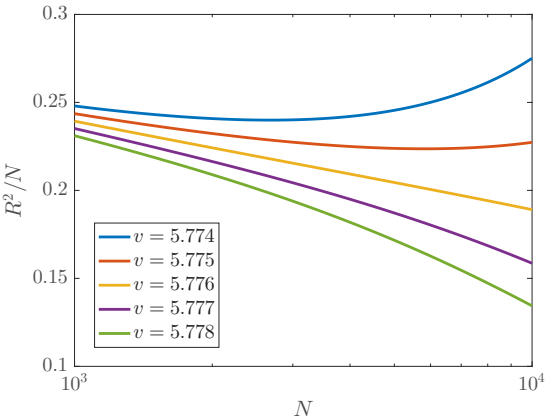

FIG. 6. Semilogarithmic plot of the scaled squared end-to-end distance R^2, as a function of polymer length N for an attractive point located inside a rectangular wedge ($\theta_0 = \pi/4$), as depicted in Fig. 4(a) for geometry "1," with Boltzmann weights v ranging from 5.774 to 5.778 (top to bottom).

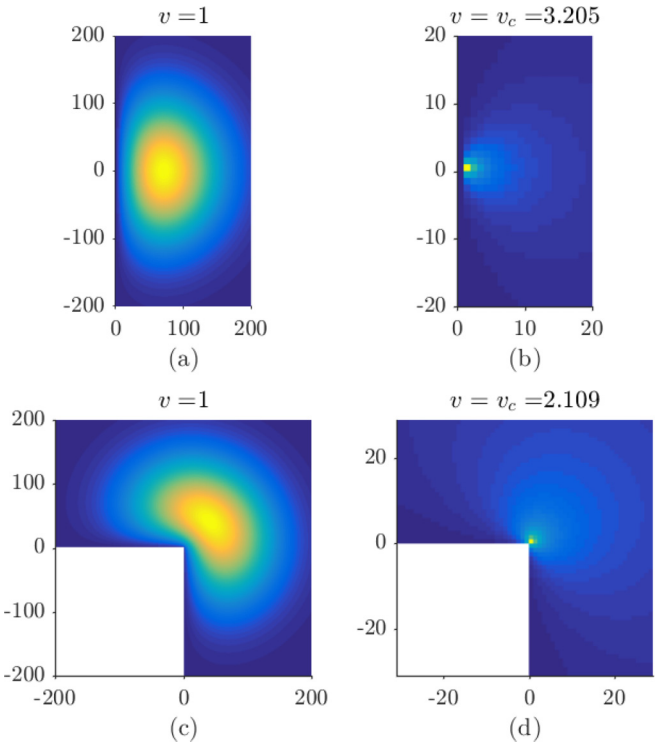

FIG. 7. Probability density of a polymer end-point position $\mathbf{r}$ for $N = 10^4$, near a flat surface [$\theta_0 = \pi/2$, panels (a) and (b)], and outside a rectangular wedge [$\theta_0 = 3\pi/4$, panels (c) and (d)]. [See geometries of type "1" in Figs. 4(b) and 4(c).] In the absence of attraction ($v = 1$) the distribution is broad with maximum at a distance $\sim\sqrt{N}$ away from the anchor point of the polymer [panels (a) and (c)], while at $v = v_c$ [panels (b) and (d)] it is centered on the anchor point.

$v = v_c$, shown in Figs. 7(b) and 7(d), the distribution is still broad but remains centered on the attracting site to which the polymer is anchored, as expected from Eq. (24), decaying as a power law cutoff at a distance of order $\sqrt{N}$. For $v > v_c$ the distributions are still centered on the attracting site, but the correlation length ξ which cuts off the power law decreases with increasing v, as will be discussed in the next section.

We analyzed $\tilde{\mathcal{Z}}_{\rm tot}$ and R^2 for all geometries depicted in Fig. 4, obtaining a set of critical values v_c that depend on both the opening semiangle θ_0, and on the specific discrete realization of the wedge. The values of v_c for all eight cases are plotted in Fig. 8. We expect v_c to decrease with increasing θ_0, and find results that qualitatively resemble that of a continuous circular well. For each value of θ_0 there is a difference between the two possible realizations on a lattice, in variants denoted "1" and "2" in Fig. 4, with the variant that has more nearest-neighbor repulsive sites, n, requiring a stronger attraction (larger v_c) to confine the polymer.

VI. CRITICAL BEHAVIOR ON A LATTICE

Figure 9 depicts on a logarithmic scale the numerically measured R^2 for several values of N as a function of $v - v_c$ close to the transition point. For each θ_0 we identify a linear segment corresponding to a power law dependence of R^2, with possible logarithmic corrections. For large N the

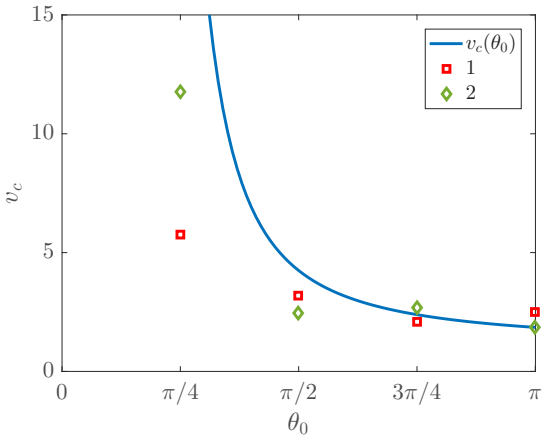

FIG. 8. Critical attractive strength v_c for four values of θ_0, and for lattice realizations "1" (squares) and "2" (diamonds) depicted in Fig. 4. For comparison, the solid line shows the continuum result for a circular well, with $v_c \equiv \exp(U_c/2d)$.

power law regime is broader and is cut off when R^2 reaches values of order of N. The graphs represent rather different geometries of the wedge, ranging from a polymer confined inside a rectangular wedge ($\theta_0 = \pi/4$), to outside a needle-like barrier ($\theta_0 = \pi$). Dashed lines indicate the theoretically predicted forms from the solution of the continuous potential well in Eq. (20). Note that, as in Eq. (21), we measure R^2 and not ξ. Thus for the polymer inside a rectangular wedge with $m = 2$, there is a logarithmic correction to the relation between R^2 and ξ^2, leading to the expectation of $R^2 \sim |(v - v_c)[c + \ln(v - v_c)]|^{-1}$. The fit in graph (a) in Fig. 9 uses $c = -4.6$. For the case of a flat line, as in variant "1" in Fig. 4(b), $m = 1$ and the relation between R^2 and $v - v_c$, has a logarithmic term

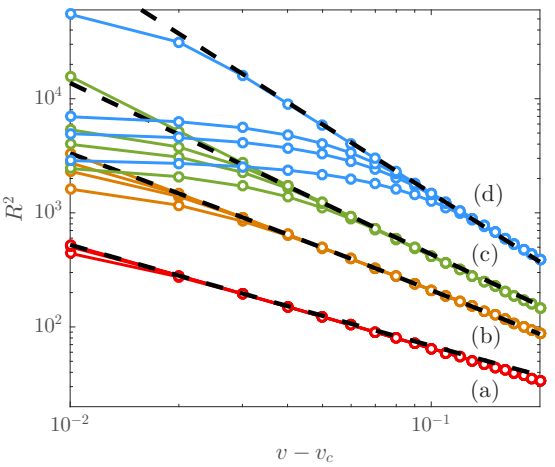

FIG. 9. Logarithmic plots of the mean squared end-to-end distance R^2 as a function of $v - v_c(\theta_0)$; different bundles of graphs correspond to different θ_0 realized by type "1" lattice variants in Fig. 4 as indicated by the legends: (a) $\pi/4$, (b) $\pi/2$, (c) $3\pi/4$, and (d) π. Each bundle combines four different values of $N = 4 \times 10^3$, 7×10^3, 10^4, and 10^5 (bottom to top). The dashed lines represent the anticipated power laws or power laws corrected by logarithms, as explained in the text.

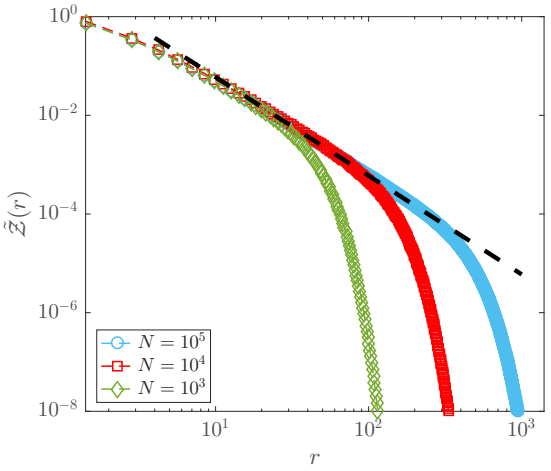

FIG. 10. Logarithmic plot of the reduced partition function in type "1" model of Fig. 4(a) as a function of distance r along the diagonal, for (left to right) $N = 10^3$, 10^4, and 10^5. All curves have slope -2 for $r \ll \sqrt{N}$ as indicated by the dashed line.

originating in the expression for ξ in Eq. (20), resulting in $R^2 \sim |c + \ln(v - v_c)|/(v - v_c)$. The fit in graph (b) in Fig. 9 uses $c = -1.6$. Finally, the wedges of type "1" in Figs. 4(c) and 4(d) exhibit a simple power law scaling on $v - v_c$ with exponents of $-3/2$ and -2, respectively, as shown in graphs (c) and (d) in Fig. 9. The match between the numerical results and theoretical predictions is quite good, although the limited range of N introduces some systematic errors: for example, for the needle-like barrier, direct measurement of the slope gives -1.95 rather than -2, as the discreteness of the lattice combined with limited N introduces finite-size effects such as a slight effective reduction of the angle θ_0, and similar corrections of order $1/\sqrt{N}$. We repeated the calculations also for variants of type "2" in Fig. 4, and despite the shifts in the positions of v_c, the results were practically indistinguishable from those in Fig. 9.

We further used the numerical results to check the validity of Eq. (24) for the behavior of $\tilde{\mathcal{Z}}(\mathbf{r_0},\mathbf{r})$ at the transition point v_c. Figure 10 displays the weight of polymers ending at a distance r from the corner of a rectangular wedge. The expected power-law scaling with exponent $-m = -2$ is clearly observed. [For proper comparison one must replace N' in the exponent in Eq. (24) by $N/4$ where N is the number of iterations used in the simulation.] However, the curves for different N do not show an increase as $N^{m-1} = N$, for fixed $r \ll \sqrt{N}$, as predicted by Eq. (24). Such a power law increase is expected *exactly* at $v = v_c$, switching to a power-law decrease as $N^{\gamma-1} = N^{-m/2} = N^{-1}$ for $v < v_c$. Thus, a small shift in v can change the behavior between power-law increase and power-law decrease. In both cases there is no exponential growth with N as occurs for $v > v_c$. The simulations are not sufficiently sensitive to locate the exact position of v_c. Indeed, the very choice of putative v_c for Fig. 10 was guided by consideration that $\tilde{Z}_{\rm tot}$ is approximately constant over the studied range of N, likely leading to a value slightly below the true v_c.

VII. DISCUSSION

In this work we studied the adsorption transition of a (phantom) polymer to the corner of a (repulsive) wedge. The scale-free nature of the geometry leads to critical exponents that depend on the opening semiangle θ_0 of the wedge: At the transition point the probability density of the end point decays as a power law $\sim r^{-m}$ with $m = \pi/2\theta_0$. On approaching the desorption point, the localization length ξ diverges with with an exponent of $1/2$ for acute and obtuse angles, then continuously increasing to one with increasing θ_0 for reflex angles. These results for $d = 2$ are equally valid for an ideal polymer near a wedge with an attractive edge in $d = 3$. Once self-avoidance is introduced, the two-dimensional solution is no longer applicable, since a self-avoiding polymer, as well as Θ polymer, cannot be adsorbed to a finite volume. However, in $d = 3$ the adsorption transition of a self-avoiding and Θ polymer to a wedge with adsorbing edge, as in Fig. 1, is expected to be qualitatively similar, with albeit different θ_0-dependent exponents.

The scale-free geometry studied in this work combines objects of different dimensionality: a zero-dimensional area of attraction with a one-dimensional repulsive surface. In $d = 3$ we can consider a richer class of scale-free objects (points, lines, planes, cones, pyramids, etc.), and more combinations of zero-, one-, and two-dimensional entities. Each one of these components can be either repulsive or attractive, and we expect to have competing and coexisting adsorption transitions. For $d = 3$ the adsorption transition problem can be expanded to more realistic self-avoiding and Θ polymers.

ACKNOWLEDGMENTS

This work was supported by the National Science Foundation under Grant No. DMR-1708280 (M.K.) and the Israel Science Foundation Grant No. 453/17 (Y.K.).

[1] E. Eisenriegler, K. Kremer, and K. Binder, J. Chem. Phys. **77**, 6296 (1982).
[2] K. Binder, in *Phase Transitions and Critical Phenomena*, edited by C. Domb and J. L. Lebowitz (Academic Press, London, 1983), Vol. 8, pp. 1–144.
[3] K. De'Bell and T. Lookman, Rev. Mod. Phys. **65**, 87 (1993).
[4] S. Livne and H. Meirovitch, J Chem. Phys. **88**, 4498 (1988).
[5] H. Meirovitch and S. Livne, J. Chem. Phys. **88**, 4507 (1988).
[6] H. Meirovitch and I. Chang, Phys. Rev. E **48**, 1960 (1993).
[7] E. Eisenriegler, *Polymers Near Surfaces* (World Scientific, Singapore, 1993).
[8] T. Vrbová and S. G. Whittington, J. Phys. A.: Math. Gen. **31**, 3989 (1998).
[9] G. Rychlewski and S. G. Whittington, J. Stat. Phys. **145**, 6611 (2011).
[10] P.-G. de Gennes, *Scaling Concepts in Polymer Physics* (Cornell University Press, Ithaca, NY, 1979).

[11] E. J. Janse van Rensburg, *The Statistical Mechanics of Interacting Walks, Polygons, Animals and Vesicles*, 2nd ed. (Oxford University Press, 2015).
[12] P.-G. de Gennes, Rep. Prog. Phys. **32**, 187 (1969).
[13] A. A. Gorbunov, E. B. Zhulina, and A. M. Skvortsov, Polymer **23**, 1133 (1982).
[14] A. Hanke, J Phys.: Condens. Matter **17**, S1731 (2005).
[15] T. M. Birshtein and O. V. Borisov, Polymer **32**, 916 (1991).
[16] T. M. Birshtein and O. V. Borisov, Polymer **32**, 923 (1991).
[17] A. Hanke, E. Eisenriegler, and S. Dietrich, Phys. Rev. E **59**, 6853 (1999).
[18] E. Ben-Naim and P. L. Krapivsky, J. Phys. A **43**, 495008 (2010).
[19] M. F. Maghrebi, Y. Kantor, and M. Kardar, Europhys. Lett. **96**, 66002 (2011).
[20] M. F. Maghrebi, Y. Kantor, and M. Kardar, Phys. Rev. E **86**, 061801 (2012).
[21] Y. Kantor and M. Kardar, Phys. Rev. E **96**, 022148 (2017).
[22] F. W. Wiegel, *Introduction to Path-Integral Methods in Physics and Polymer Science* (World Scientific, Singapore, 1986).
[23] W. F. Buell and B. A. Shadwick, Am. J. Phys. **63**, 256 (1995).
[24] L. D. Landau and E. M. Lifshitz, *Quantum Mechanics (Non-Relativistic Theory)*, 3rd ed., Course of Theoretical Physics No. 3 (Elsevier, Amsterdam, 2005).
[25] K. R. Brownstein, Am. J. Phys. **68**, 160 (2000).
[26] K. Chadan, N. N. Khuri, A. Martin, and T. T. Wu, J. Math. Phys. **44**, 406 (2003).
[27] M. M. Nieto, Phys. Lett. A **293**, 10 (2002).
[28] R. W. Robinett, Eur. J. Phys. **24**, 231 (2003).
[29] NIST Digital Library of Mathematical Functions http://dlmf.nist.gov/.
[30] M. Abramowitz and I. A. Stegun, editor, *Handbook of Mathematical Functions*, 10th ed. (National Bureau of Standards, Washington, DC, 1972).
[31] A. Laforgia and M. A. Muldoon, J. Math. Anal. Appl. **98**, 470 (1984).
[32] Y. Hammer and Y. Kantor, Phys. Rev. E **89**, 022601 (2014).
[33] T. Bickel, C. Jeppesen, and C. M. Marques, Eur. Phys. J. E **4**, 33 (2001).
[34] M. Breidenich, R. R. Netz, and R. Lipowsky, Europhys. Lett. **49**, 431 (2000).
[35] I. Jensen, W. G. Dantas, C. M. Marques, and J. F. Stilck, J. Phys. A **46**, 115004 (2013).
[36] Y. Hammer and Y. Kantor, J. Chem. Phys. **141**, 204905 (2014).
[37] N. Alfasi and Y. Kantor, Phys. Rev. E **91**, 042126 (2015).